PAPER

Fluorescent molecularly imprinted polymer nanocomposite for solid-phase extraction and fluorimetric determination of hydrochlorothiazide

Ahmed S. Abo Dena, [iD] *[ab] Mariam Dhaou[ac] and Ibrahim M. El-Sherbiny [iD] *[a]

We report herein a fluorescent molecularly imprinted polymer (FMIP) for the solid-phase extraction (SPE) and fluorimetric determination of hydrochlorothiazide (HCTZ) in water. The FMIP is based on fluorescent polystyrene nanoparticles embedded within a molecularly imprinted polyaniline (PANI) matrix. The operational adsorption parameters such as the initial HCTZ concentration, incubation time and the solution pH were found to influence the removal efficiency. At optimum conditions, a high adsorption capacity of the FMIP was found (2.08 mg g^{-1}). Evidence of the adsorption process was confirmed by the change in the FMIP physicochemical properties measured by FTIR absorption spectroscopy and electron microscopy. Based on the regression R^2 values and the consistently low values of the adsorption statistical error functions, equilibrium data were best fitted to both Freundlich and Temkin isotherms. Moreover, the pseudo-second-order kinetic model described the adsorption kinetics, and the mechanism of the adsorption process was explained by the intraparticle diffusion model. Upon studying adsorption thermodynamics, negative ΔG values (-26.18 kJ mol^{-1} at room temperature) were obtained revealing that the adsorption process is spontaneous. Interestingly, the maximum adsorption capacity was obtained at 298 K, pH 7.0, and using a high HCTZ concentration, thus revealing the suitability of the proposed FMIP for easy and fast SPE of HCTZ. The FMIP showed an imprinting factor of 1.19 implying the selectivity over the corresponding FNIP. Eventually, the proposed FMIP was successfully applied to the spectrofluorimetric determination of HCTZ in aqueous samples with %recovery values close to 100%.

Introduction

Pharmaceutical compounds represent an environmental concern because of their existence in aquatic ecosystems within the effluents of pharmaceutical factories, leading to ecotoxicological effects. In addition, due to their extensive use for disease treatments in humans and animals, wastewater discharges into municipal systems present high concentrations of these compounds and their metabolites, leading to harmful effects on the environment, that could reach humans and animals *via* direct or indirect ways.[1] Hydrochlorothiazide (HCTZ), a common pharmaceutical compound (Scheme 1), is one of the oldest members of thiazide diuretics, which comprises two sulfonamide groups. The IUPAC name of HCTZ is 6-chloro-1,1-doxo-3,4-dihydro-2*H*-1,2,4-benzothiadiazine-7-sulfonamide. Despite its poor water solubility at room temperature (20–

30 mg L^{-1}), HCTZ remains one of the most dangerous water contaminants. It has been extensively used for the treatment of hypertension and cardiovascular morbidity,[2–4] oedema (caused by using certain medications such as oestrogen and corticosteroids), liver damage, swelling (due to kidney problems), muscle spasms, erectile dysfunction, and photosensitivity. In fact, as drugs are designed to produce pharmacological effects using low doses, they are capable of producing negative ecotoxicological as well as health effects on humans and other organisms when introduced to the environment even at low concentrations.

Due to their serious toxicological effects, wastewater contamination with pharmaceutical residues is a topic of great interest. Numerous water purification techniques are being

[a]Nanomedicine Laboratories, Centre for Materials Science (CMS), Zewail City of Science and Technology, 6 October City, 12578, Giza, Egypt. E-mail: ielsherbiny@ zewailcity.edu.eg; aabdelmawgoud@zewailcity.edu.eg

[b]Pharmaceutical Chemistry Department, National Organization for Drug Control and Research (NODCAR), Giza, Egypt

[c]Laboratory of Materials for Energy and Environment, and Modelling, Faculty of Science, University of Sfax, 3000, Sfax, Tunisia

Scheme 1 Chemical structure of HCTZ.

used; for instance, advanced oxidative degradation, electro-coagulation, membrane filtration, biochemical degradation, flocculation, chemical precipitation, reverse osmosis, electrodialysis and ion-exchange methods. Some studies have focused on the development of methods such as solid-phase extraction (SPE), solid-phase microextraction (SPME), and ultrasound-assisted dispersive liquid–liquid microextraction. Alternatively, adsorption is considered one of the most promising techniques owing to the ease of operation, low cost, and design flexibility. It presents a profitable, robust and universal approach for the elimination of toxic pharmaceutical residues from aquatic environments.

In recent years, the adsorption of water pollutants using molecularly imprinted polymers (MIPs) has attracted the attention of researchers. MIPs are versatile and robust polymers that can be easily tailored for fast and selective separation,[5] chemical sensing,[6] catalysis,[7,8] biological imitation,[9] and other fields due to the specific active sites or cavities they have, that provide selective recognition of small or large molecules, high binding capacity, and stable physiochemical properties.[10] Moreover, considering their specific adsorption power, MIPs have a great potential as carrier materials in clinical and pharmaceutical applications such as the analysis of biological samples and drug delivery.[11] The MIP is firstly prepared by a simple polymerization or copolymerization method in the presence of the target template molecules (i.e. analyte molecules) and a crosslinking agent under appropriate reaction conditions. The template molecules are then removed leaving recognition cavities complementary in shape, size, and coordination geometry to themselves.[12]

The selection of the functional monomers is critical to the molecular recognition ability. Not only does an appropriate functional monomer enhance the affinity of the template molecules to the MIP, but also it reduces the nonspecific adsorption to enhance its specificity towards the template molecules.[13,14] In previous studies, polyaniline (PANI)-based MIP exhibited good selective adsorption[15] to template molecules such as benzophenone-4,[16] ascorbic acid,[17] 2,4-dinitrophenol,[18] antibiotic residues,[19] acrylamide,[20] and horseradish peroxidase.[21] PANI is a synthetic semi-crystalline organic polymer that does not require high-temperature polymerization conditions nor a crosslinking agent. The recent interest in PANI applications is due to its unique properties including the ease of fabrication, low cost, high stability, chemical resistance and high electrical conductivity. Because of these unique properties, PANI is a potential candidate as a MIP adsorbent for wastewater purification.[22,23] The integration of a fluorescent material with PANI-based MIPs results in excellent dual-use MIP materials. These materials can be used for the SPE as well as the fluorimetric determination of the specific analytes for which they are tailored.

In this regard, the current study aims at tailoring and synthesizing a fluorescent MIP (FMIP)-based adsorbent for the SPE and spectrofluorimetric determination of HCTZ in aqueous media. The proposed FMIP is based on a nanocomposite of polystyrene nanoparticles (PSNPs) and molecularly imprinted PANI nanofibers. The PSNPs were incorporated into the PANI matrix in order to provide the MIP with light-emitting properties that can be useful in spectrofluorimetric determination of HCTZ. The synthesized nanocomposite was characterized by thermogravimetric analysis (TGA), differential scanning calorimetry (DSC), scanning electron microscopy (SEM), high-resolution transmission electron microscopy (HR-TEM), Fourier-transform infrared absorption spectroscopy (FTIR), dynamic light scattering (DLS) and zeta potential measurements. The effect of the adsorbent dose and the HCTZ initial concentration on the adsorption capacity of the FMIP was studied. Moreover, adsorption isotherms, kinetic models and the thermodynamics of the adsorption process were thoroughly investigated. To the best of our knowledge, this is the first study to apply a dual-use FMIP material for SPE and spectro-fluorimetric determination of HCTZ in its aqueous solutions.

Materials and methods

Materials

HCTZ and methyclothiazide (MTZ) standards were obtained from the Egyptian Drug Authority, Egypt. For the synthesis of the molecularly imprinted PANI, aniline (Sigma-Aldrich, Germany), acetonitrile (Sigma-Aldrich, Germany) and potassium persulfate (PPS, Laborchemie Apolda GmbH, Germany) were used. Acetic acid (Honeywell International Inc., USA) and anhydrous hydrochloric acid ($\geq$99.5%) was purchased from Sigma-Aldrich, Germany. All the used chemicals and reagents are of analytical grade, and they were used without any further purification prior to the experimental procedure. HPLC grade dichloromethane (DCM) and methanol were used during the course of the experimental work.

Preparation of PSNPs

The synthesis of PSNPs was achieved through the following steps. First, accurately weighed 2.0 g of polystyrene (PS) were dissolved in 20 mL of dichloromethane (Sigma-Aldrich, Germany). Thereafter, this solution was dropped onto 100 mL of 3% (w/v) polyvinyl alcohol (PVA, Acros Organics, USA) with continuous vigorous mechanical stirring until the whole amount of dichloromethane is evaporated. Subsequently, the produced PSNPs were collected by centrifugation at 9000 rpm for 10 min. The collected amount of PSNPs was washed several times, and then left to dry overnight at 60 °C in a vacuum oven.

Preparation of FMIP

Accurately weighed 100 mg of PSNPs were well dispersed in 10 mL of HCl (1 M) containing 90 µL of aniline via magnetic stirring. In addition, an acetonitrile/HCl (5 : 10, v/v) solution containing 0.297 g of dissolved HCTZ were added to the above mixture, and the resulting mixture was agitated in an ice bath at 5 °C. Thereafter, 10 mL of PPS solution (20 mg mL^{-1} in 1 M HCl) was dropped onto the above mixture with continuous stirring. The obtained MIP/PSNPs composite (i.e. FMIP) was collected and washed twice with distilled water, and then dried in ambient temperature. The appearance of a dark green colour indicates the formation of the emeraldine salt of PANI (Fig. 1). The FNIP was prepared by following the same procedure
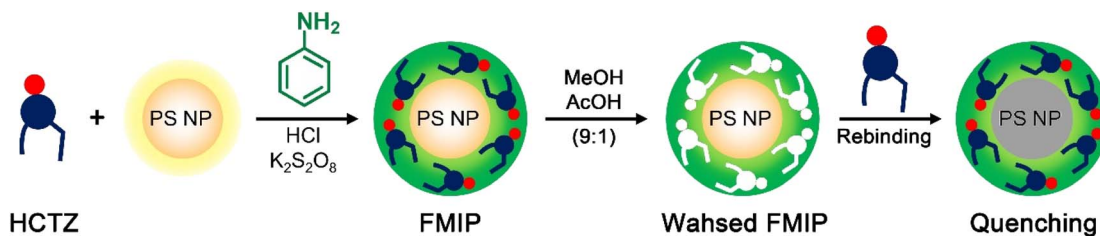
Fig. 1 Schematic representation of the preparation steps of FMIP and its use in the SPE and fluorimetric determination of **HCTZ**.

without the addition of **HCTZ**. The obtained FMIP was collected from the suspension *via* centrifugation at 9000 rpm for 10 min, and then washed thrice with distilled water. Subsequently, the incorporated **HCTZ** molecules were removed from the FMIP *via* repeated washing with a mixture of methanol and 1% acetic acid solution (9 : 1, v/v) until no **HCTZ** could be detected spectrophotometrically at 272 nm. Thereafter, the resultant solid was washed several times with methanol to remove the excess acetic acid. The resulting FMIP was left overnight to dry at room temperature. In order to reduce any systematic errors, the prepared FNIP was handled in a similar manner.

Materials characterization

The FTIR spectra of the FMIP as well as the FNIP were recorded over the spectral window 4000–400 cm^{-1} with the aid of a Nicolet iS10 Mid infrared ATR-FTIR spectrometer (Thermoscientific, USA). Electron micrographs were recorded using a JEOL JEM-2100 HR-TEM (USA) for investigating the morphology of the prepared nanocomposites. The DLS measurements were carried out with the aid of a Malvern instrument.

Adsorption measurements. The efficiency of the prepared sorbents for the removal of **HCTZ** from solutions was determined by soaking 20 mg of the sorbent in 10 mL of **HCTZ** solution of an appropriate concentration at room temperature, and then the solution was stirred for a specified period. The concentration of **HCTZ** that remained in the solution after soaking (C_f) with the sorbent was measured by recording the absorbance at 272 nm. Working drug solutions (10–50 mg L^{-1}) were freshly prepared prior to each experiment by diluting a 1×10^3 mg L^{-1} **HCTZ** stock solution with bidistilled water.

The effect of pH on the drug adsorption was studied by using working solutions of different pH values (pH 2–10) adjusted by a 0.1 mol L^{-1} solution of hydrochloric acid or sodium hydroxide. The pH of the prepared solutions was measured using a JENCO 6173 pH meter.

The specific adsorption ratio was calculated from the following formula (eqn (1)):[23]

$$A(\%) = \frac{(C_i - C_f)}{C_i} \times 100 \quad (1)$$

where C_i and C_f are the initial and equilibrium concentrations of **HCTZ** (mg L^{-1}), respectively.

The adsorption capacities of the prepared FMIP and FNIP were calculated from eqn (2):[23]

$$q = \frac{(C_i - C_f)}{m} \times V \quad (2)$$

where q (mg g^{-1}) is the adsorption capacity, V is the solution volume in litres, and m is the adsorbent mass in grams.

The imprinting factor (IF) was calculated as the ratio between the binding capacity of FMIP and that of the corresponding FNIP using eqn (3):

$$IF = \frac{q_{FMIP}}{q_{FNIP}} \quad (3)$$

Adsorption kinetics and isotherms. Kinetic models such as the pseudo-first-order (PFO),[24] pseudo-second-order (PSO),[25] the Weber–Morris, the intraparticle diffusion (IPD),[26] and Elovich[27] models were applied to demonstrate and assess the adsorption rate constants. Also, various adsorption isotherms such as Langmuir, Freundlich, Temkin, Dubinin–Radushkevich (D–R), Halsey, and Javanovic were used in order to understand the retention/release of the drug molecules by/from the FMIP adsorbent. The formulae and the corresponding constants of the kinetic and isotherm models are summarized in Table 1.

An adsorption isotherm is a plot that describes the adsorption equilibrium at constant pH and temperature.[23,28] The Langmuir (eqn (7)), Freundlich (eqn (8)), and Temkin (eqn (9)) isotherms are the most common and traditional isotherm models used. These models were applied in the present study in order to investigate the release/retention of **HCTZ** from/by the FMIP in aqueous solution.

Adsorption thermodynamics and adsorbent dose. Adsorption thermodynamic parameters were calculated by incubating 0.2 g of the FMIP in 2 mL of a 50 mg L^{-1} **HCTZ** solution for the equilibration time. The experiment was repeated at different test solution temperatures (300–330 K). Subsequently, the adsorption equilibrium constant (K_a) was calculated at the studied temperatures from eqn (13):[23,28]

$$K_a = C_{ad}/C_e \quad (13)$$

where K_a is the distribution constant, which is equal to the adsorption equilibrium constant, C_{ad} is the concentration of adsorbed **HCTZ**, and C_e is the equilibrium concentration of **HCTZ**. The obtained K_a values were used to calculate the adsorption thermodynamic parameters (ΔH and ΔS) from Van't Hoff equation (eqn (14)) *via* plotting ln K_a *vs.* 1/T[23,28]

$$\ln K_c = \ln K_a = \frac{-\Delta H}{RT} + \frac{\Delta S}{R} \quad (14)$$

Table 1 Kinetics and isotherm models for the removal of HCTZ from water using the as-prepared FMIP

Model	Equation	Variables and constants	
PFO	$q = q_e(1 - e^{k_1 t})$	q_e: equilibrium capacity (mg g^{-1}) q_t: adsorption capacity (mg g^{-1}) at time t (min) k_1: rate constant (min^{-1}) V: solution volume (L) m: adsorbent mass (g)	(4)
PSO	$\dfrac{t}{q} = \dfrac{1}{k_2 q_e^2} + \dfrac{t}{q_e}$	k_2: rate constant (g mg^{-1} min^{-1})	(5)
IPD	$q = k_p(t)^{1/2} + c$	k_p: IPD rate constant (mg g^{-1} min$^{-1/2}$) C: constant	(6)
Langmuir	$\dfrac{C_e}{q_e} = \dfrac{1}{bq_{max}} + \left(\dfrac{1}{q_{max}}\right)C_e$	b: Langmuir's constant (L mg^{-1}) q_{max}: maximum adsorption capacity (mg g^{-1})	(7)
Freundlich	$\ln q_e = \ln k_F + \left(\dfrac{1}{n}\right)\ln C_e$	k_F: Freundlich constant n: strength of adsorption	(8)
Temkin	$q_e = \left(\dfrac{RT}{b_T}\right)\ln k_1 + \left(\dfrac{RT}{b_T}\right)\ln C_e$	b_T: Temkin's adsorption constant R: the universal gas constant (0.00813 kJ mol^{-1} K^{-1}) K_T: equilibrium binding constant (mol L^{-1}) T: absolute temperature (K)	(9)
D–R	$\ln q_e = \ln q_m - \beta\varepsilon^2$ $\varepsilon = RT \ln\left(1 + \dfrac{1}{C_e}\right)$ $E = \left(\dfrac{1}{2\beta}\right)^{0.5}$	β: the activity coefficient ε: Polanyi potential E: adsorption energy	(10)
Halsey	$q_e = \exp\left[\dfrac{\ln K_H - \ln C_e}{n_H}\right]$	K_H: Halsey isotherm constant n_H: Halsey isotherm exponent	(11)
Jovanovic	$\ln q_e = \ln q_{max} - K_J C_e$	K_J: Jovanovic isotherm constant	(12)

Additionally, the change in Gibbs free energy (ΔG) was calculated from eqn (15).[23,28]

$$\Delta G = \Delta H - T\Delta S \qquad (15)$$

where ΔH is the enthalpy change, ΔS is the entropy change, R is the universal gas constant and T is the absolute temperature.

Spectrofluorimetric determination of HCTZ

A standard curve was plotted by measuring the fluorescence emission intensity of solutions containing increasing concentrations of **HCTZ** and a fixed amount of the prepared FMIP using a Shimazdu RF-6000 Spectrofluorimeter, Japan. The concentrations of the used solutions are in the range of 2.86–22.86 μmol L^{-1}. The emission spectra were recorded in the spectral range of 200–400 nm. For the validation of the proposed method, authentic sample solutions of **HCTZ** were prepared by spiking bidistilled water with different amounts of **HCTZ**, and then the samples were analysed using the above procedure and the recovery values as well as all the analytical parameters were calculated.

Results and discussion

This section will cover the results obtained from the characterization techniques along with the optimization procedure of the adsorption conditions of the drug under investigation (**HCTZ**) onto the suggested FMIP. In addition, the results of the spectrofluorimetric analytical method used for the determination of **HCTZ** in aqueous solution using the same FMIP are introduced herein.

FTTR analysis

The FTIR spectrum of **HCTZ** (Fig. 2) shows characteristic absorption bands at 2986, 1551, 1413, 1272, 1169, 1019, 970, 828, and 674 cm^{-1} that can be assigned to C–H stretching, C–O stretching, C=N stretching, pyridine stretching, ring vibration, ring breathing, P–O–C, P=S stretching, and C–Cl stretching, respectively.[33]
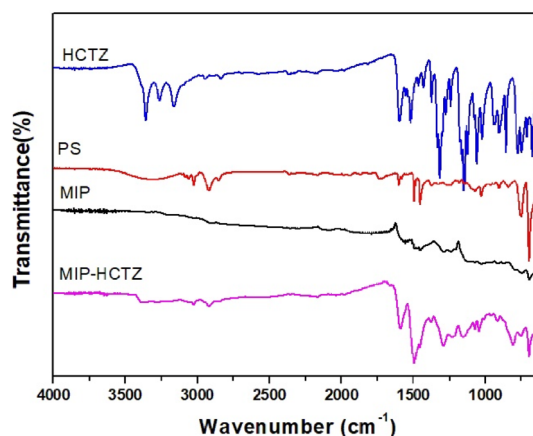
Fig. 2 FTIR spectra of **HCTZ**, PS, washed FMIP and unwashed FMIP (MIP-HCTZ).

In the case of pure PS, the FTIR spectrum revealed a characteristic band at about 756 and 698 cm^{-1} corresponding to the C–H. The sharp bands appearing at about 1600, 1492, and 1452 cm^{-1} indicate the presence of aromatic C=C. In addition, the presence of absorption bands at 2921 and 2848 cm^{-1} may correspond to the existence of a methylene group. The presence of hydroxyl groups was confirmed by the appearance of a strong broad band at 3650–3000 cm^{-1}.[34]

For the FMIP, the absence of the hydroxyl band at 3500–3300 cm^{-1} negates the presence of bound water molecules; indicating that the FMIP sample was well dried prior to the FTIR measurement. The broad absorption band positioned at a wavenumber higher than 2000 cm^{-1} is a typical band of conducting PANI. Moreover, the strong broad band positioned around 1000 cm^{-1} is attributed to the bond vibrations of –NH$^+$=, Q=NH$^+$–B, or B–NH$^+$–B, where B is the benzenoid unit, and Q is the quinonoid unit. This band also confirms the dihedral angles distribution between B and Q rings as well as the presence of positively charged moieties in the PANI chains, thus confirming the formation of emeraldine salt.[35] The large similarity between the FTIR spectrum of **HCTZ** and that of the unwashed FMIP (MIP-HCTZ) confirms the successful binding of **HCTZ** to the PANI backbone. For instance, all the characteristic **HCTZ** absorption bands appear at 3360, 3161, 2944, 1591, 1380, 1013, 753, 552, and 540 cm^{-1} in the MIP-HCTZ spectrum.

DLS measurements and electron microscopy

The average particle size of the as prepared PSNPs was investigated with dynamic light scattering measurement (Fig. 3a), and was found to be 284.4 nm. To further confirm the particle size of PSNPs obtained from DLS measurements, and to explore their morphology, the nanoparticles were imaged with transmission electron microscopy. As depicted in Fig. 3b, the prepared PSNPs exhibit a well-defined spherical shape and a homogeneous size of less than 100 nm. It is worth mentioning that the high hydrophobicity of the PSNPs prevents their agglomerations, that is why no aggregates could be seen in the TEM image. It is obvious from these two characterization techniques that there is a slight difference between the two recorded particles sizes since the size obtained from DLS measurements appears slightly larger than its TEM counterpart. In order to justify this, it is necessary to explain the principle of DLS measurements. A rapid photon counter is used in a DLS experiment to track time-dependent variations in the scattered light signal. The hydrodynamic radius may be computed using the macromolecule or particle's diffusion coefficient, which can be obtained by DLS measurements. Accordingly, the DLS instrument does not have the ability to discriminate single particles from aggregates, and hence it provides an average particle size for both, which is usually larger than the size of the particles imaged by TEM.

Contact time and adsorption kinetics

One of the important relevant parameters that control the transfer of adsorbate molecules (and the build-up of charges) from the bulk to the pores or the active sites of the adsorbent (FMIP in the present study) is the contact time. The influence of the contact time was studied over the period of 30–150 min *via* measuring the absorbance of the solutions at 272 nm. As illustrated in Fig. 4b, a rapid adsorption was observed in the first 30 min due to the high attractive forces between the FMIP's active sites and the **HCTZ** molecules. Thereafter, after 70 min, there was no significant increase in the amount of adsorbed **HCTZ**. After 90 min, the removal efficiency reached a plateau, meaning that the FMIP surface became saturated and the system has attained equilibrium. Therefore, the optimum contact time of the FMIP with the **HCTZ** solution was selected at 75 min. A fast diffusion towards the surface of the FMIP was followed as a result of the participation of the
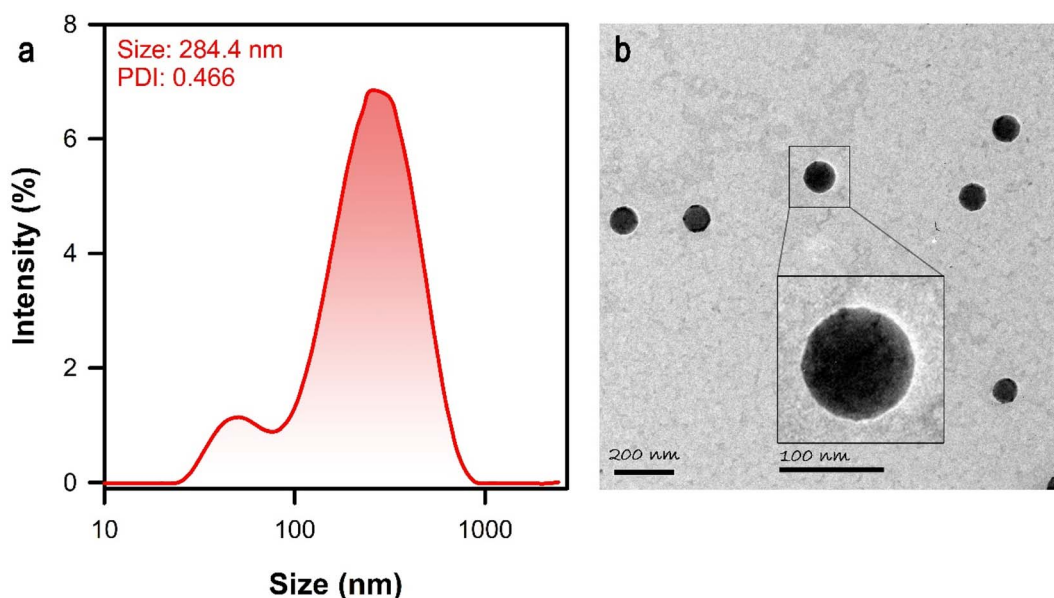

Fig. 3 Dynamic light scattering measurement (a) and TEM image (b) of PSNPs.
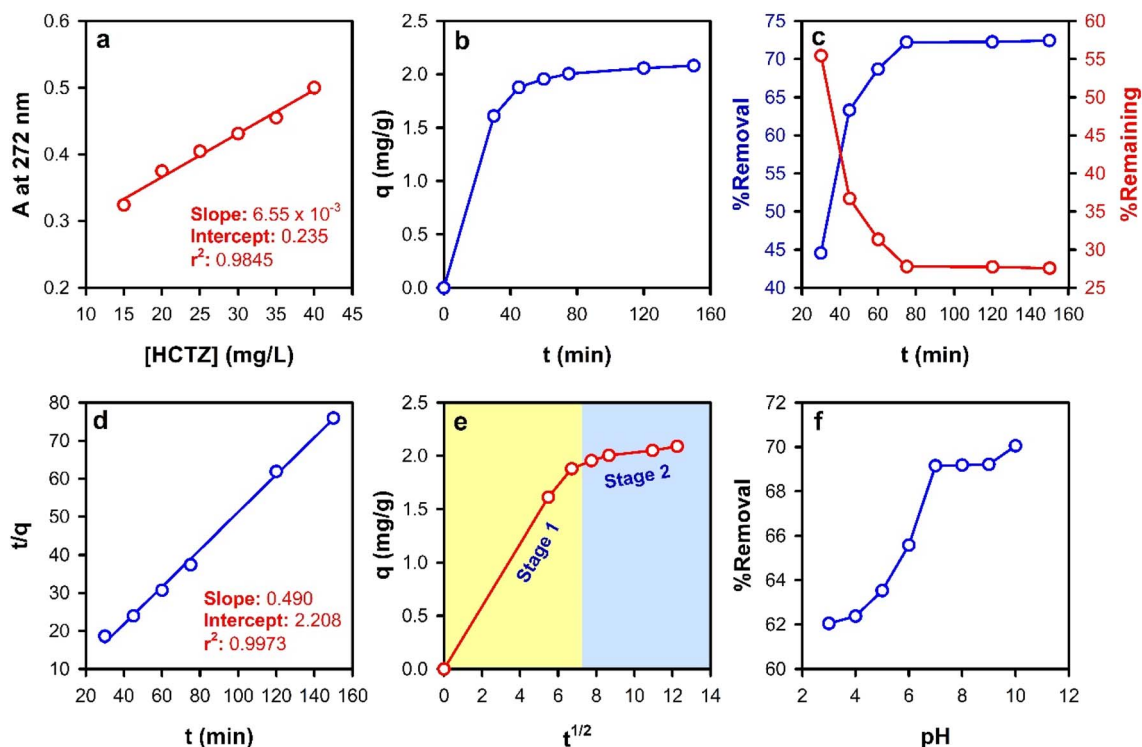
Fig. 4 (a) standard curve of **HCTZ** in aqueous medium at 272 nm, (b) influence of the contact time on the FMIP capacity, (c) influence of the contact time on **HCTZ** removal, (d) PSO kinetic model for the adsorption of **HCTZ** onto the FMIP, (e) IPD kinetic model, and (f) the influence of the solution pH on the removal of **HCTZ** using the FMIP. All data points are an average of three repetitions with a standard deviation in the range of 0.06−1.4.

functional groups until equilibrium was attained, where about 72% removal efficiency was achieved. The change in the rate of **HCTZ** ion removal might be due to the fact that initially all the FMIP active sites were vacant. Afterwards, the number of the available active sites decreases continuously leading to a corresponding decrease in the rate of adsorption. The mean adsorption capacity of the proposed FMIP was found to be 2.0 mg g^{-1}.

The adsorption kinetic models are basically used to understand the mechanism of the adsorption process by fitting the obtained experimental data to the theoretical kinetic models such as PFO, PSO, Elovich, fractional power (power function), and the IPD. The application of the PSO kinetic model yielded a perfect fit to the experimental results obtained for the adsorption of **HCTZ** ions onto the FMIP at the tested concentration (50 mg L^{-1}), with a coefficient of determination of $R^2 = 0.995$. The experimental value of q_e is usually higher than the value calculated from the PSO kinetic model. Curiously, q_e and k_2 (the adsorption rate constant) values calculated from the PSO kinetic model were found to be 2.04 mg g^{-1} and 5×10^{-3} g mg^{-1} min^{-1}, respectively (Fig. 4d). Interestingly, it is obvious from the q_e values that the experimental and PSO-calculated values are almost identical. Fitting of the experimental data to the PSO kinetic model implies that the chemisorption of **HCTZ** is the rate-limiting step, and the removal of **HCTZ** molecules from bulk solution is due to the physicochemical interactions between **HCTZ** and the FMIP surface.

The IPD model explains the removal mechanism of **HCTZ** by FMIP, as well to the PFO and the PSO models. Fig. 4e displays a two-stage adsorption process. Stage 1 resembles the intraparticle or pore diffusion, where the adsorbate molecules percolate into the interior of the adsorbent particles. This stage involves the diffusion of the adsorbate from the bulk through the liquid film that surrounds the surface of the adsorbent particles. On the other hand, stage 2 represents the equilibrium stage, where the adsorption and desorption processes of **HCTZ** molecules onto/from the FMIP occur at comparable rates. The calculated values of the rate constant (k_{IPD}) are 0.28 and 0.027 mg g^{-1} $min^{-1/2}$ for stage 1 and stage 2, respectively, demonstrating that the rate of adsorption is faster in case of the former. This can be also confirmed by comparing the values of the intercepts. Larger intercept values imply a greater effect of the boundary layer. The obtained intercept values are 0.008 mg g^{-1} and 1.75 mg g^{-1} for

Table 2 The results of the applied kinetic models for the adsorption of HCTZ onto the synthesized FMIP

Kinetic model	Parameters	Calculated value
PFO	k_1 (L min^{-1})	−0.063
	q_e (mg g^{-1})	2.17
PSO	k_2 (L min^{-1})	0.364
	q_e (mg g^{-1})	2.040
IPD	K_{IPD} (stage 1) (mg g^{-1} $min^{-1/2}$)	0.28
	K_{IPD} (stage 2) (mg g^{-1} $min^{-1/2}$)	0.027

stage 1 and stage 2, respectively. The results of the applied adsorption kinetic models are summarized in Table 2.

Influence of pH

The effect of pH on the adsorption of **HCTZ** molecules onto the fabricated FMIP was studied and the obtained results are shown in Fig. 4f. The solution pH was varied to cover a range of 2–10. The ionic mobility, the degree of ionization, and the surface chemistry of the FMIP were influenced by the changes in solution pH. The test was conducted at the equilibrium contact time (75 min) using 20 mg of FMIP and 50 mg L^{-1} solution of **HCTZ** as an initial **HCTZ** concentration. At low pH values, protonation of PANI (emeraldine salt) results in charging of the FMIP surface with a large number of positive charges.[23] Simultaneously, the amino groups of the **HCTZ** molecules get protonated forming positively charged quaternary ammonium groups. Accordingly, the repulsion between the **HCTZ** molecules and the surface of the adsorbent hinders the attachment of the **HCTZ** molecules to their specific active sites, and the rate of adsorption increases as the pH becomes more basic. The maximum adsorption capacity was attained at a solution pH of 7.0, where about 69% of the initial **HCTZ** amount was removed.

Adsorption isotherms

The adsorption equilibrium data was evaluated with the commonly employed isotherm models such as Langmuir, Freundlich, Temkin, Dubinin–Radushkevich, Halsey and Jovanovic. Fig. 5 depicts the original linearized mathematical expressions of the applied isotherm models mentioned above.

The influence of increasing the initial **HCTZ** concentration on the adsorption capacity of the FMIP was used to calculate the IF of the synthesized FMIP (Fig. 5a and b). This was achieved by comparing the maximum adsorption capacity recorded for the FMIP with that recorded for the corresponding FNIP, as
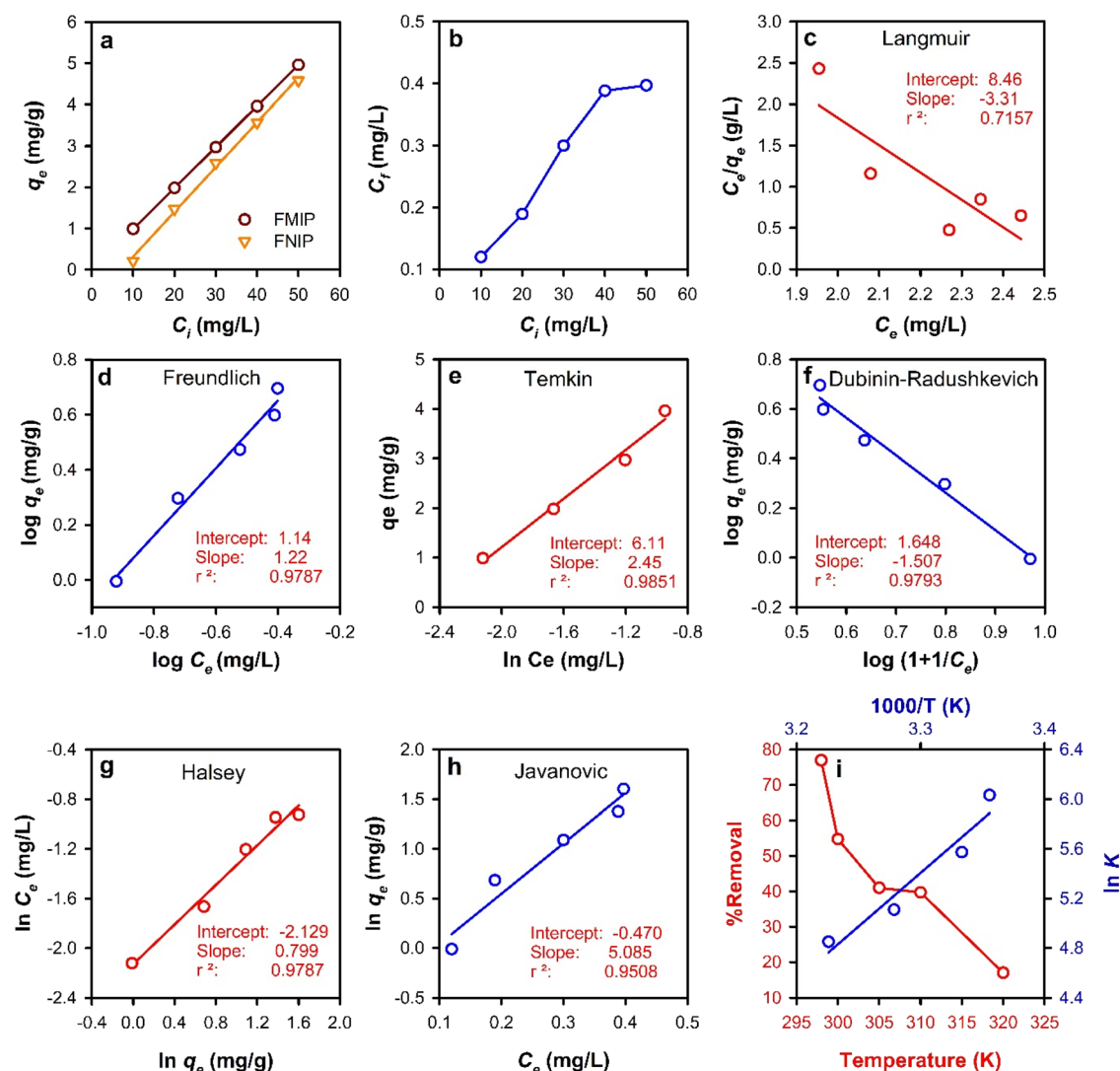

Fig. 5 (a) Dependence of adsorption capacity on the initial **HCTZ** concentration, (b) increase in the amount of the remaining **HCTZ** with increasing the initial **HCTZ** concentration, (c) Langmuir isotherm, (d) Freundlich isotherm, (e) Temkin isotherm, (f) Dubinin–Radushkevich isotherm, (g) Halsey isotherm, (h) Javanovic isotherm, and (i) thermodynamics and the effect of temperature on the adsorption of **HCTZ** onto the synthesized FMIP. All data points are an average of three repetitions with a standard deviation in the range of 0.06–1.4.

Table 3 Calculated parameters for the applied adsorption isotherm models for the SPE of HCTZ using the suggested FMIP adsorbent

Isotherm model	Parameter symbol	Parameter value
Langmuir	q_L (mg g^{-1})	0.301
	K_L (L mg^{-1})	0.391
	R_L	0.0188–0.0761
	R^2	0.7157
Freundlich	K_F	3.131
	n_F	1.220
	R^2	0.9787
Temkin	b_T	1024
	B (J mol^{-1})	12.128
	A (L g^{-1})	2.447
	R^2	0.9851
D–R	Q_{D-R} (mg g^{-1})	0.221
	K_{D-R}	−1.146
	E	−1.514
	R^2	0.9793
Halsey	n_H	1.251
	K_H	2.129
	R^2	0.9787
Javanovic	Q_J (mg g^{-1})	5.084
	K_J	1.599
	R^2	0.9508

explained in the Materials and methods section (Adsorption measurements). The calculated IF was found to be 1.19 indicating the higher selectivity of the FMIP over the FNIP towards the HCTZ molecules.

As shown in Fig. 5c, the Langmuir model has not demonstrated the best fitting to the experimental data of HCTZ adsorption onto the FMIP. The same can be noticed in the case of the Jevanovic model (Fig. 5h). This conclusion was drawn by the obtained low values of R^2 which attained 0.75 and 0.95, respectively. The calculated values of q_{max} and b_L were found to be −0.301 mg g^{-1} and −0.391, respectively. The negative value of q_{max} indicates the inadequacy of the Langmuir isotherm to describe the adsorption of HCTZ molecules onto the FMIP surface.

Unlikely, the linear correlation coefficient of Freundlich isotherm plot ($R^2 = 0.978$) suggests that Freundlich isotherm fits the experimental data due to the multilayer adsorption to the heterogeneous surface (Fig. 5d). The characteristic parameters of the Freundlich isotherm model are the K_F (adsorption coefficient) and the n_F values which were found to be 3.13 and 1.22, respectively. The small value of n_F indicates that the

Table 4 Thermodynamic parameters of HCTZ adsorption on FMIP

T (K)	K_a	Slope	Intercept	ΔH (J mol^{-1})	ΔS (J mol^{-1} K^{-1})	ΔG (kJ mol^{-1})
298	416.34	4.85	−10.55	−40.32	−87.71	−26.181
300	263.28					−26.356
305	165.66					−26.795
310	127.80					−27.723
320	125					−28.111

adsorption of more HCTZ molecules becomes difficult/unfavourable as the amount of the adsorbed HCTZ increases on the FMIP surface, thus interpreting the relatively long time required for attaining the equilibrium. A better fit to the experimental results, with an R^2 value of 0.9851, was observed in the case of Temkin isotherm. The theoretical adsorption capacities were in good agreement with the experimental values for both the Langmuir and Freundlich isotherm models (Table 3). The values of the separation factor (R_L) indicate the adsorption nature to either unfavourable or favourable, it is unfavourable if $R_L > 1$, linear if $R_L = 1$, favourable if $0 < R_L < 1$, and reversible if $R_L = 0$. The calculated values of R_L ranged from 0.0188 to 0.0761 indicating that the adsorption process is favourable.

Table 5 Analytical parameters and analytical applications of the proposed FMIP in the assay of water samples spiked with different amounts of HCTZ

Analytical parameters	
Linear range, mol L^{-1}	3.8×10^{-6}–3.1×10^{-5}
Limit of detection (LOD), mol L^{-1}	1.14×10^{-6}
Limit of quantification (LOQ), mol L^{-1}	3.8×10^{-6}
Intercept (a)	1.000
Slope (b)	0.013
R^2	0.9949

Recovery study			
Taken (µg)	Found (µg)	Recovery (%)	SD
Spiked distilled water samples			
1.0	1.00	100.00	0.45
2.0	2.10	105.0	0.84
4.0	3.95	98.75	0.46
6.0	6.34	105.7	0.76
8.0	8.23	102.9	0.24
Spiked tap water samples			
2	2.05	102.5	0.32
4	4.13	103.3	0.27
8	7.94	99.25	0.51
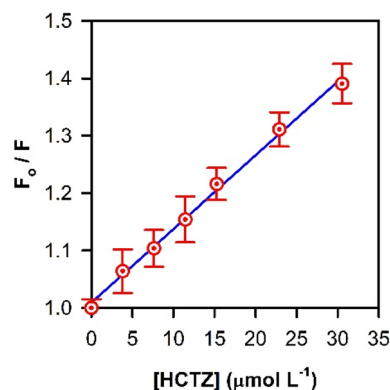
Fig. 6 Standard plot for the determination of HCTZ using the proposed FMIP-based fluorimetric sensor. F and F_o are the fluorescence intensities of the test and blank samples, respectively.

Table 6 Analytical parameters and analytical applications of the proposed FMIP in the assay of water samples spiked with different amounts of HCTZ

Analytical method	LOD ($\mu g\ mL^{-1}$)	Linear range ($ng\ mL^{-1}$)	Reference
MIP-based spectrofluorometry	339.4	$11.31–9.2 \times 10^3$	This work
Capillary electrophoresis	—	$2 \times 10^4–6 \times 10^5$	29
LC/TMS	0.230	0.78–200	30
Electrochemical sensor	357.3	$8.9 \times 10^2–2.2 \times 10^3$	31
Electrochemical sensor	5.955	$14.9–5.95 \times 10^4$	32
Time-resolved chemiluminescence	340.0	$5 \times 10^2–3 \times 10^4$	33
	160.0		
HPLC/fluorescence	20.00	$20–1 \times 10^3$	34

Temkin isotherm (Fig. 5e) assumes a linear variation of the heat of adsorption with the degree of overlap. Since the heat of adsorption is a function of temperature of all molecules in the surface layer of the adsorbent, the plot decreases linearly as a result of increasing the surface coverage. The value of the constant b determines the type of the sorption process. When b_T value is less than 8×10^4, this indicates a physical adsorption. Though, the value of the term RT/b_T, also termed as B, gives information about the heat of adsorption. B-Values less than $8\ kJ\ mol^{-1}$ indicate a weak interaction between the adsorbate molecules and the adsorbent surface. The calculated b_T value is 1024 and the B value was found to be $12.128\ J\ mol^{-1}$. These values were obtained by plotting q_e versus $\ln C_e$, which showed an R^2 value of 0.985. From regression coefficient values, it is obvious that both Temkin and Freundlich isotherms demonstrated the best fitting to the experimental results; thus confirming the involvement of physical adsorption in the governing mechanism of the removal of **HCTZ** by the proposed FMIP adsorbent.

Adsorption thermodynamics and the effect of temperature

To build up a perspective about the mechanism of **HCTZ** adsorption at the surface of the FMIP, the adsorption equilibrium constant (K_a) was calculated at different test solution temperatures, and then the thermodynamic parameters were subsequently obtained. The calculated negative values of ΔG at the studied temperatures indicate that **HCTZ** adsorption onto the FMIP is a spontaneous process, and **HCTZ** molecules tend to stay in the stationary phase near to the FMIP surface. Normally, physisorption is indicated by standard free energy change values (ΔG) ranging from 0 to $20\ kJ\ mol^{-1}$, whereas these of chemisorption range from 80 to $400\ kJ\ mol^{-1}$. The calculated values of ΔG (Table 4) confirm that the adsorption process takes place by physisorption. Therefore, the involvement of the imprinted active sites on the FMIP surface is highly acceptable, which coincides with the calculated IF value (~1.19).

Analytical applications

In order to investigate the ability of the proposed FMIP material to respond to changes in the **HCTZ** concentration, spiked water samples were prepared and analysed for the concentration of

HCTZ using the proposed spectrofluorimetric assay method, and the analytical parameters and the recovery percentages were calculated (Table 5).

The calibration curve (Fig. 6) used for the determination of the **HCTZ** concentration in the above-mentioned spiked samples showed linearity over the concentration range of $3.8 \times 10^{-6}–3.1 \times 10^{-5}\ mol\ L^{-1}$ and the recovery values ranged from 98.75 to 105.7%. In addition, the R^2 value of the standard plot is 0.9949. Moreover, it is worth mentioning that a low limit of detection (LOD) was obtained ($1.14 \times 10^{-6}\ mol\ L^{-1}$) indicating the sensitivity of the proposed analytical method. The low values of standard deviation (SD, 0.24–0.84) indicate the precision of the proposed procedure, while recovery values near to 100% indicate its accuracy. To investigate the selectivity of the present fluorimetric sensor, samples of **HCTZ** were spiked with methyclothiazide in a ratio of 1 : 10 (**HCTZ** : MTZ) and then the samples were analysed using the calibration curve procedures described herein. The results indicate that despite the great structural similarity between **HCTZ** and MTZ, the proposed fluorimetric sensor demonstrated a high selectivity towards **HCTZ** as revealed by the obtained accurate recovery value (97.3%).

The applicability of the investigated sensor to real water sample analysis was evaluated *via* analysing multiple tap water samples spiked with **HCTZ**. The obtained high recovery and low standard deviation values (Table 5) indicate the accuracy and precision of the proposed analytical method. Table 6 compares the analytical parameters of the proposed analytical method in the present work with those of some other reported methods.

Conclusion

Here, we studied the successful adsorption of **HCTZ** ions on the proposed FMIP. The synthesized FMIP material was characterized using the suitable characterization techniques such as FTIR spectroscopy, electron microscopy, and dynamic light scattering. Investigating the interaction of the **HCTZ** molecules with the surface functional groups of the FMIP revealed that the adsorption process takes place *via* a physisorption mechanism. The adsorption followed a pseudo-second-order kinetics and the highest SPE efficiency was attained at room temperature and at pH 7.0; thus allowing for facile and fast separation and analysis of **HCTZ**. The FMIP was successfully applied to the

determination of **HCTZ** in aqueous samples *via* the spectro-fluorimetric technique. The novelty of this work is that the proposed FMIP material has a dual function, since it can be used simultaneously for both the SPE extraction and the assay of **HCTZ** in its aqueous samples. This property allows for the fast analysis of **HCTZ** in complex samples which require sample pre-treatment procedure such as separation and/or masking of the undesired interfering species.

Author contributions

Ahmed S. Abo Dena: conceptualization, methodology, investigation, formal analysis, data curation, visualization, writing-review and editing. Mariam Dhaou: methodology, investigation, writing-original draft. Ibrahim M. El-Sherbiny: supervision, resources, project administration, writing-review and editing.

Conflicts of interest

There are no conflicts to declare.

Acknowledgements

Notes and references

1 S. Dineva, K. Uzunova, V. Pavlova, E. Filipova, K. Kalinov and T. Vekov, *J. Hum. Hypertens.*, 2019, **33**, 766–774.

2 K. M. Neff and J. J. Nawarskas, *Cardiol. Rev.*, 2010, **18**, 51–56.

3 The fifth report of the Joint National Committee on Detection, Evaluation, and Treatment of High Blood Pressure (JNC V), *Arch. Intern. Med.*, 1993, **153**, 2, 154–183.

4 Mortality after 10 1/2 years for hypertensive participants in the Multiple Risk Factor Intervention Trial, *Circulation*, 1990, **82**, 5, 1616–1628.

5 A. Asfaram, M. Ghaedi and K. Dashtian, *Ultrason. Sonochem.*, 2017, **34**, 640–650.

6 J. W. Lowdon, H. Diliën, P. Singla, M. Peeters, T. J. Cleij, B. van Grinsven and K. Eersels, *Sens. Actuators, B*, 2020, **325**, 128973.

7 T. Kubo and K. Otsuka, *J. Pharm. Biomed. Anal.*, 2016, **130**, 68–80.

8 X. Xin, H. Liu, N. Zhong, M. Zhao, D. Zhong, H. Chang, B. Tang, Y. He, C. Peng and X. He, *Sens. Actuators, B*, 2022, **357**, 131468.

9 G. K. Ali and K. M. Omer, *Talanta*, 2022, **236**, 122878.

10 W. Zhang, X. She, L. Wang, H. Fan, Q. Zhou, X. Huang and J. Z. Tang, *Materials*, 2017, **10**(5), 475–490.

11 B. Sellergren and C. J. Allender, *Adv. Drug Delivery Rev.*, 2005, **57**, 1733–1741.

12 L. Chen, S. Xu and J. Li, *Chem. Soc. Rev.*, 2011, **40**, 2922–2942.

13 H. Ran, Z. Lin, C. Hong, J. Zeng, Q.-H. Yao and Z.-Y. Huang, *J. Photochem. Photobiol., A*, 2019, **372**, 260–269.

14 L. Chen, X. Wang, W. Lu, X. Wu and J. Li, *Chem. Soc. Rev.*, 2016, **45**, 2137–2211.

15 H. Freundlich, *J. Phys. Chem.*, 1907, **57**, 385–470.

16 C. Ayadi, A. Anene, R. Kalfat, Y. Chevalier and S. Hbaieb, *Colloids Surf., A*, 2019, **567**, 32–42.

17 A. K. Roy, V. S. Nisha, C. Dhand and B. D. Malhotra, *J. Mol. Recognit.*, 2011, **24**, 700–706.

18 A. Mehdinia, M. Ahmadifar, M. O. Aziz-Zanjani, A. Jabbari and M. S. Hashtroudi, *Analyst*, 2012, **137**, 4368–4374.

19 V.-P. Vu, Q.-T. Tran, D.-T. Pham, P.-D. Tran, B. Thierry, T.-X. Chu and A.-T. Mai, *Vietnam J. Chem.*, 2019, **57**, 328–333.

20 A. Drame, Š. Trafela and K. Ž. Rožman, *Proceedings*, 2019, **15**, 37.

21 P. S. Pidenko, S. A. Pidenko, Y. S. Skibina, A. M. Zacharevich, D. D. Drozd, I. Y. Goryacheva and N. A. Burmistrova, *Anal. Bioanal. Chem.*, 2020, **412**, 6509–6517.

22 Á. Villabona-Ortíz, K. J. Figueroa-Lopez and R. Ortega-Toro, *Sustainability*, 2022, **14**, 3640.

23 H. Saad, F. A. Nour El-Dien, N. E. A. El-Gamel and A. S. Abo Dena, *RSC Adv.*, 2021, **11**, 39768–39780.

24 H. Dai, Y. Huang, H. Zhang, L. Ma, H. Huang, J. Wu and Y. Zhang, *Carbohydr. Polym.*, 2020, **230**, 115599.

25 M. Ateia, D. E. Helbling and W. R. Dichtel, *ACS Mater. Lett.*, 2020, **2**, 1532–1544.

26 S. Mignardi, L. Archilletti, L. Medeghini and C. De Vito, *Sci. Rep.*, 2020, **10**, 2436.

27 K. C. Bedin, A. C. Martins, A. L. Cazetta, O. Pezoti and V. C. Almeida, *Chem. Eng. J.*, 2016, **286**, 476–484.

28 H. Saad, F. A. Nour El-Dien, N. E. A. El-Gamel and A. S. Abo Dena, *RSC Adv.*, 2022, **12**, 25487–25499.

29 S. Hillaert and W. Van den Bossche, *J. Pharm. Biomed. Anal.*, 2003, **31**, 329–339.

30 F. Liu, Y. Xu, S. Gao, J. zhang and Q. Guo, *J. Pharm. Biomed. Anal.*, 2007, **44**, 1187–1191.

31 M. C. G. Santos, C. R. T. Tarley, L. H. Dall'Antonia and E. R. Sartori, *Sens. Actuators, B*, 2013, **188**, 263–270.

32 H. Beitollahi, M. Hamzavi and M. Torkzadeh-Mahani, *Mater. Sci. Eng., C*, 2015, **52**, 297–305.

33 J. A. Murillo Pulgarín, A. Alañón Molina and G. Pérez-Olivares Nieto, *Anal. Chim. Acta*, 2004, **518**, 37–43.

34 A. Hemdan, N. F. Al-Tannak and E. H. Mohamed, *J. Sep. Sci.*, 2022, **45**, 824–831.

35 V. Suendo, Y. Lau, F. Hidayat, M. Reza, A. Qadafi and A. Rochliadi, *Phys. Chem. Chem. Phys.*, 2021, **23**, 7190–7199.